Inorganic Chemistry

Article

pubs.acs.org/IC

A Highly Efficient White Light $(Sr_3,Ca,Ba)(PO_4)_3Cl:Eu^{2+}$, Tb^{3+}, Mn^{2+} Phosphor via Dual Energy Transfers for White Light-Emitting Diodes

Xi Chen,[†] Pengpeng Dai,*[,†] Xintong Zhang,*[,†] Cong Li,[†] Shan Lu,[‡] Xiuli Wang,[§] Yan Jia,[†] and Yichun Liu[†]

[†]Center for Advanced Optoelectronic Functional Materials Research, and Key Laboratory for UV-Emitting Materials and Technology of Ministry of Education, [‡]School of Life Sciences, and [§]School of Geographic Sciences, Northeast Normal University, 5268 Renmin Street, Changchun 130024, China

Supporting Information

ABSTRACT: A series of single-phased $(Sr_{3-x-y-z}Ca_yBa)(PO_4)_3Cl$ (SCBPO_Cl):-xEu^{2+}, yTb^{3+}, zMn^{2+} phosphors were synthesized by high-temperature solid-state reaction, and luminescent properties of these phosphors were investigated by means of photoluminescence and microcathode luminescence (μ-CL). Under UV excitation, white-light emission was obtained from triactivated SCBPO_Cl phosphors via combining three emission bands centered at 450, 543, and 570 nm contributed by Eu^{2+}, Tb^{3+}, and Mn^{2+}, respectively. White-light emission with the three emission bands is further demonstrated in the fluorescence microscope images, CL spectrum, and μ-CL mappings, which strongly confirm that the luminescence distribution of as-prepared SCBPO_Cl:xEu^{2+}, yTb^{3+}, zMn^{2+} phosphors is very homogeneous. Both spectral overlapping and lifetime decay analyses suggest that dual energy transfers, that is, $Eu^{2+}\rightarrow Tb^{3+}$ and $Eu^{2+}\rightarrow Mn^{2+}$, play key roles in obtaining the white emission. The International Commission on Illumination value of white emission as well as luminescence quantum yield (51.2−81.4%) can be tuned by precisely controlling the content of Eu^{2+}, Tb^{3+}, and Mn^{2+}. These results suggest that this single-phased SCBPO_Cl:xEu^{2+}, yTb^{3+}, zMn^{2+} phosphor may have a potential application as a near-UV convertible white-light emission phosphor for phosphor-converted white light-emitting diode.

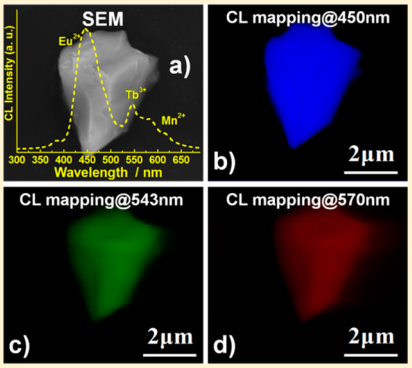

1. INTRODUCTION

The use of phosphor-converted white light-emitting diodes (WLEDs) for general lighting are attracting extensive research and commercial interest because of their long lifetime, high luminous efficiency, low power consumption, and environmentally friendly characteristics.[1−3] Currently, the commercially available WLEDs are based on a blue chip with yellow-emitting phosphor (YAG:Ce). This approach can generate a relatively cool white light that is uncomfortable for indoor lighting due to red deficiency.[4,5] White light conversion from near-UV light emitting diodes (NUVLEDs) by use of tricolor phosphors are considered to be a more promising route to cover indoor lighting needs for their better color rendering ability. Unfortunately, strong cascade excitation among tricolor phosphors causes significant color altering and decreases the luminous efficiency of WLEDs.[6,7] Moreover, different thermal quenching behavior of each component in tricolor phosphors and the complicated coating technology involved are still problems hard to tackle.[8,9] In these regards, a single-phased direct white-emitting phosphor pumped by NUVLEDs should be a good choice for phosphor-converted WLEDs, since they exhibit definite advantages, such as improved color stability, better reproducibility, and a simplified fabrication process.[10−12]

Recently, several strategies were proposed to fabricate a single-phased white-emitting phosphor for WLEDs, including semiconducting nanocrystals,[13] inorganic microporous materials,[14] light-emitting complexes,[15,16] and multiple activators codoped compound.[17] One of the most promising approaches for generating white light from a single-phased compound is to dope multiactivators; namely, a rare earth sensitizer and multiple activators (rare earth or transition metal) are codoped into a crystalline matrix, such as $Eu^{3+}/Tm^{3+}/Tb^{3+}$,[18] $Eu^{2+}/Eu^{3+}/Tb^{3+}$,[19] $Eu^{3+}/Tb^{3+}/Dy^{3+}$[20], and $Ce^{3+}/Tb^{3+}/Mn^{2+}$ ions.[21] It is because rare earth and transition metal ions have rich energy levels that researchers have greater flexibility in designing novel luminescent materials, using the principle of the energy transfer (ET), for different applications. As is well-known, trivalent Tb^{3+} is an ideal green-emitting activator, showing sharp line emissions at 488, 545, and 583 nm. Seven-coordinated or octahedral-coordinated Mn^{2+} can yield a broad-band orange-red or red emission, which covers almost the whole red emission area from 560 to 650 nm.[22,23] Thus, Tb^{3+} and Mn^{2+} ions are frequently selected as green- and red-emitting activator in luminescent materials. However, both the green emission, originating from the f−f transition of Tb^{3+}, and the red emission, originating from the d−d transition of Mn^{2+}, are forbidden transitions and have very weak excitation in the

Received: November 19, 2013
Published: March 21, 2014

   dx.doi.org/10.1021/ic402870p | Inorg. Chem. 2014, 53, 3441−3448

NUV region.[24,25] As an effective activator, the Eu^{2+} ion can not only efficiently absorb NUV light to emit blue light but can also act as an efficient sensitizer for Tb^{3+} and Mn^{2+} activators. Therefore, it is highly expected to obtain a white-light phosphor pumped by NUV light in an appropriate host by dual ETs of Eu^{2+} to Tb^{3+} and Mn^{2+}, as follows, $Eu^{2+}\rightarrow Tb^{3+}$ and $Eu^{2+}\rightarrow Mn^{2+}$.

Apatite-type alkaline-earth halophosphates with the general formula of $M_5(PO_4)_3Cl$ (M = Ca, Sr, Ba) as host of luminescence materials have been widely investigated because of the flexibility of host lattice, good thermal stability, cheap raw materials, and simple synthesis conditions.[26−28] In the $M_5(PO_4)_3Cl$ structure, there are two types of cationic sites (M1 and M2), which are the 6-fold coordinated 4f sites and 7-fold coordinated 4h sites, respectively.[29] Both sites are suitable and easily accommodate a great variety of foreign cations, for example, rare earth ions, transition metal ions, and alkaline earth ions with different ionic radii, which make it possible to design a novel luminescence material. $(Sr_3,Ca,Ba)(PO_4)_3Cl$ is a host showing excellent luminescence properties when doped with rare earth or transition metal ions.[26] Herein, a series of Eu^{2+}, Tb^{3+}, and Mn^{2+} tridoped $(Sr_3,Ca,Ba)(PO_4)_3Cl$ phosphors are synthesized by high-temperature solid-state reactions. As expected, a bright white light can be realized in SCBPO_Cl:-$x$$Eu^{2+}$, $y$$Tb^{3+}$, $z$$Mn^{2+}$ powders by utilizing the principle of dual ETs under excitation at 365 nm. Their luminescence properties and dual ET mechanisms are discussed in detail in regard to the photoluminescence excitation, lifetime decay, fluorescence microscopic images, cathode luminescence (CL) spectra, and microcathode luminescence (μ-CL) mappings .

2. EXPERIMENTAL SECTION

2.1. Materials and Synthesis. Samples were synthesized by a conventional high-temperature solid-state reaction using stoichiometric amounts of $SrHPO_4$ (99.9%), $SrCO_3$ (99.0%), $CaHPO_4{\cdot}2H_2O$ (98%), $CaCO_3$ (99.9%), $SrCl_2{\cdot}6H_2O$ (99.5%), $BaCO_3$ (99.9%), Eu_2O_3 (99.99%), Tb_4O_7 (99.99%), and $MnCO_3$ (99.9%). The raw materials were ground in an agate mortar. The mixtures were filled in alumina crucibles with covers and were sintered at 1100 °C for 2 h by slowly raising the temperature under a reducing CO atmosphere in a muffle furnace. The pellets prepared in this way were cooled quickly to room temperature and then ground to powders in an agate mortar for subsequent use.

2.2. Characterization. Composition and phase purity of the samples were studied by using a Rigaku D/max-2500 X-ray diffractometer (XRD) with Cu Kα radiation (λ = 1.5406 Å). The photoluminescence (PL) spectra were measured with a homemade PL measurement system that was made up of a NUVLED array (365 nm emission, full width at half-maximum (fwhm): 14 nm) as excitation source and a miniature fiber optic spectrometer (Ocean Optics USB 4000) as detector. Photoluminescence excitation (PLE) spectra of powders were measured with a FLS920 fluorescence spectrophotometer (Edinburgh Instruments, UK) equipped with a 450 W Xe lamp as excitation source and a red-sensitive photomultiplier tube (PMT, R-928) as optical detector. Fluorescence microscope images (TE-2000 Instruments; Nikon, Japan) were recorded under UV excitation at 365 nm to investigate the luminescence distribution of powder particles. The CL spectra and μ-CL mapping measurements (Mono CL 4 system; Gatan, UK) were conducted in a field emission scanning electron microscope (SEM, Quanta 250, FEI) equipped with a CL detector (blue-sensitive PMT). The phosphors were excited by electron beam under accelerating voltage of 20 kV and filament currents of 20 μA. The absolute quantum yield (QY) was analyzed with a PL quantum-efficiency measurement system (C9920−02, Hamamatsu Photonics). The WLEDs based on the NUVLED were fabricated using a mixture of silicon resin and the as-prepared white-light SCBPO_Cl:0.05Eu^{2+}, 0.3Tb^{3+}, 0.3Mn^{2+} phosphor, which was dropped onto a 400 nm UV LED chip (InvenLux, China, wavelength peak: 395−400 nm, chip size: 12 × 12 mil, forward voltage: 3.0−3.5 V, luminous power: 5−6 mW). The optical properties, including the electroluminescent spectrum and International Commission on Illumination (CIE) value of the WLEDs, were measured by a fiber optic spectrometer with an integrated sphere (Ocean Optics USB 4000). All measurements were performed at room temperature.

3. RESULTS AND DISCUSSION

Figure 1a presents the XRD patterns of SCBPO_Cl:$x$$Eu^{2+}$, $y$$Tb^{3+}$, $z$$Mn^{2+}$ powders prepared by solid-state reaction. The

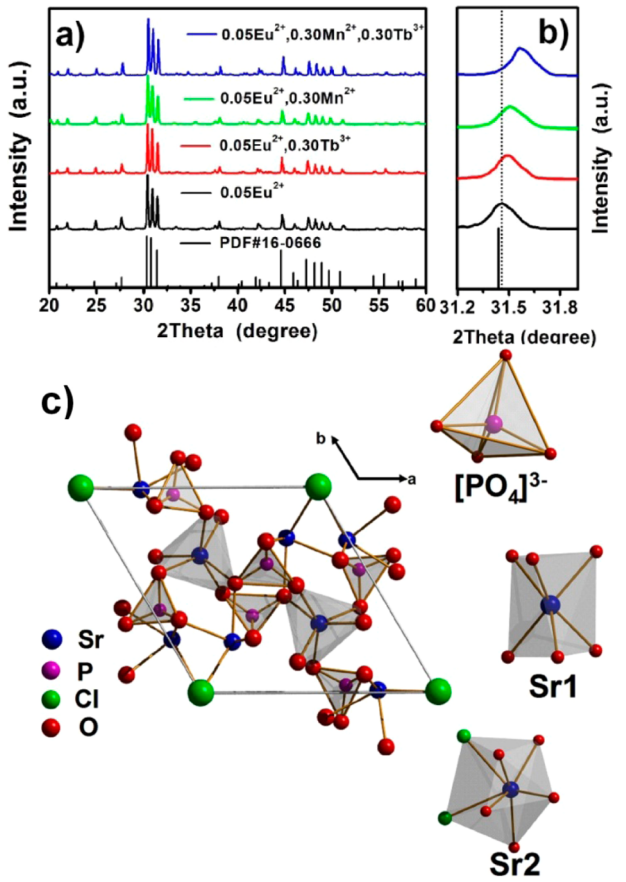

Figure 1. (a) XRD patterns of SCBPO_Cl:0.05Eu^{2+}, $y$$Tb^{3+}$, $z$$Mn^{2+}$ phosphors. The standard data for $Sr_5(PO_4)_3Cl$ (PDF#16−0666) is shown as a reference. (b) Magnified XRD patterns in the region between 31 and 32° for SCBPO_Cl:0.05Eu^{2+}, $y$$Tb^{3+}$, $z$$Mn^{2+}$ phosphors. (c) Crystal structure of $Sr_5(PO_4)_3Cl$ unit cell viewed in c-direction and the coordination environment of cation sites in $Sr_5(PO_4)_3Cl$.

XRD patterns of Eu^{2+}-doped, Eu^{2+}- and Mn^{2+}-codoped, Eu^{2+}- and Tb^{3+}-codoped, and Eu^{2+}-, Tb^{3+}-, Mn^{2+}-tridoped SCBPO_Cl samples show characteristic patterns associated with hexagonal structure (space group $P63/m$) and are coincident with the apatite-type $Sr_5(PO_4)_3Cl$ (PDF card No.16−0666). No other phase or impurity can be detected, indicating that Eu^{2+}, Tb^{3+}, and Mn^{2+} ions are completely doped in the SCBPO_Cl host lattice with no significant change in the crystal structure. However, the diffraction peaks shift slightly to the higher angle side with introduction of Tb^{3+} and Mn^{2+} ions, as shown in Figure 1b. This phenomenon indicates that partial substitution of Sr^{2+}/Ca^{2+} with Eu^{2+}, Tb^{3+}/Mn^{2+} causes a change

dx.doi.org/10.1021/ic402870p | Inorg. Chem. 2014, 53, 3441−3448

in lattice constant of the host lattice.[30] The alkaline-earth halophosphates $(Sr_3,Ca,Ba)(PO_4)_3Cl$ are isostructural to the apatite-type $Sr_5(PO_4)_3Cl$ compounds,[31] which has cell parameters of a = 9.859 Å, c = 7.206 Å, V = 606.58 Å^3, and N = 2, and their crystal structures are shown in Figure 1c. The crystal structure of $Sr_5(PO_4)_3Cl$ indicates that each cation has different coordination environments; for example, the Sr1 atom located at 4f sites is surrounded by six O atoms, with an average distance of 2.574 Å, while the Sr2 atom located at 6h sites is surrounded by five O and two Cl atoms, with an average distance of 2.717 Å.[32] Two Sr atoms are connected by tetrahedral PO_4 groups and through sharing vertices. Herein, we propose that the Ba^{2+} and Ca^{2+} ions should randomly occupy the Sr^{2+} sites in the SCBPO_Cl structure.[33] The effective ionic radii of Eu^{2+}, Tb^{3+}, Mn^{2+}, Sr^{2+}, Ca^{2+}, and Ba^{2+} are shown in Supporting Information Table S1. On the basis of the comparison of the effective ionic radii of these cations with the given coordination number, the Eu^{2+}, Tb^{3+}, and Mn^{2+} ions are expected to randomly occupy the Sr/Ca sites in the host lattice.

Figure 2 shows the PL and PLE spectra of single Eu^{2+}-doped SCBPO_Cl samples. Under excitation at 365 nm, SCBPO_-

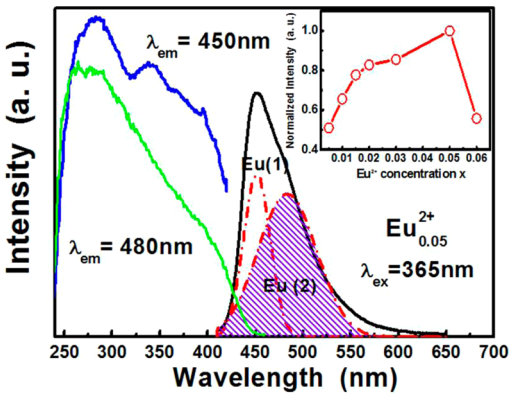

Figure 2. (a) The PL(right) and PLE(left) spectra of SCBPO_-Cl:0.05Eu^{2+} powder. The inset shows the integrated PL intensity as a function of Eu^{2+} content for SCBPO_Cl:$x$$Eu^{2+}$ under excitation at 365 nm.

Cl:Eu^{2+} powders exhibit an intense blue emission and show one asymmetric emission band peaking at 450 nm, which is ascribed to the 4f→5d transition of the Eu^{2+}. With increasing content of Eu^{2+}, the luminous intensity is dramatically intensified and reaches a maximum at an optimal content of 0.05, as shown in the inset of Figure 2. At this optimal content of 0.05, the QY of the SCBPO_Cl:0.05Eu^{2+} phosphor can reach 85% under excitation at 365 nm. The asymmetric emission band indicates that there is more than one emission center in SCBPO_Cl lattice. As shown in Figure 1c, two different Sr sites exist in the SCBPO_Cl crystal structure, that is, the 6-fold coordinated 4f sites (referred to as Sr1) and 7-fold coordinated 6h sites (referred to as Sr2). This emission spectrum thus can be deconvoluted into at least two Gaussian components peaked at 450 and 482 nm. In SCBPO_Cl:0.05Eu^{2+}, the average interatomic length between Eu^{2+} and oxygen/chlorine ($d_{Eu-O/Cl}$) is 2.574 Å for Eu^{2+} occupying the Sr1 site and 2.717 Å for the Sr2 site. In general, the bond length affects the crystal field strength significantly. Thus, we infer that the band at 450 nm, assigned to Eu (1), is occupying Sr2 sites with a weak crystal field, and the other one at 482 nm, corresponding to Eu (2), is occupying Sr1 sites with a strong crystal field.[34] Of course, Eu (2) also has contributions to this broad excitation band obtained by monitoring the 450 nm emission band, since the Eu (1) band overlaps partially with the Eu (2) band at ca. 450 nm, as shown in Figure 2. The PLE spectra are obtained by monitoring the emission at 450 and 482 nm. Both PLE spectra exhibit a broad band from 220 to 430 nm, which can be assigned to the 4f→5d transitions of Eu^{2+} ion. However, their spectral profiles are different, indicating that the two transitions originate from Eu^{2+} ions occupying two different cation sites, Sr (1) and Sr (2), which is in agreement with the PL results. Note that there is an overlap between the PLE spectrum of Eu(2) and the PL spectrum of Eu(1) in the range of 400−420 nm, which suggests the occurrence of ET from the Eu(1) to Eu(2).

Figure 3 illustrates the PL and PLE spectra of Eu^{2+}, Tb^{3+}, and Mn^{2+} single-doped SCBPO_Cl powders. The SCBPO_-

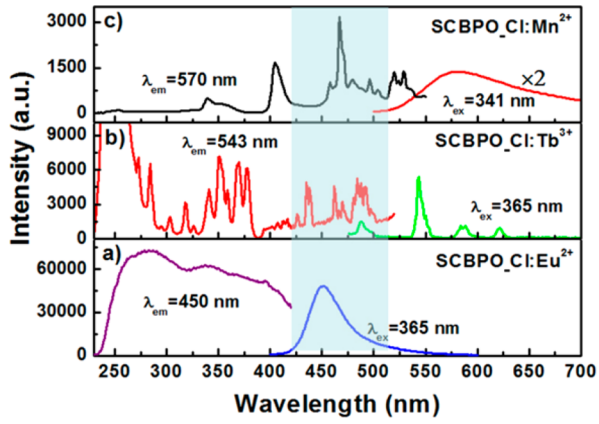

Figure 3. The PLE and PL spectra of (a) SCBPO_Cl:Eu^{2+}, (b) SCBPO_Cl:Mn^{2+}, (c) SCBPO_Cl:Tb^{3+} phosphor.

Cl:0.05Eu^{2+} powders show a bright blue light at 450 nm (λ_{ex} = 365 nm). The PLE spectrum monitored at 450 nm exhibits a broad band within 250−430 nm, covering the NUV spectral region (Figure 3a). The PL spectrum (λ_{ex} = 365 nm) of SCBPO_Cl:Tb^{3+} shows several sharp lines located at 488, 543, 585, and 621 nm, which are assigned to the $^5D_4$−$^7F_{J=6,5,4,3}$ transitions. The PLE spectrum (λ_{em} = 543 nm) of Tb^{3+} consists of several lines in the region from 370−550 nm, which correspond to the intra-4f transition of the Tb^{3+} (Figure 3b). As for the SCBPO_Cl:Mn^{2+} powders, under excitation at 341 nm, a broad-band orange-red emission at 570 nm is observed, which is assigned to the $^4T_1$→$^6A_1$ transition of Mn^{2+} and demonstrates Mn^{2+} ions occupy 7-coordinated Sr2. Monitoring the emission at 570 nm, several weak peaks are observed in the wavelength range of 350−500 nm, which can be attributed to the d−d transition of Mn^{2+} (Figure 3c). Compared to the PL result of SCBPO_Cl:Eu^{2+}, single-doped samples SCBPO_Cl:Tb^{3+}/Mn^{2+} exhibit a very weak emission under NUV excitation because of their forbidden f−f/d−d transitions in the NUV region. It is clearly seen from Figure 3a−c that the Eu^{2+} PL band overlaps well with both PLE spectra of Tb^{3+} and Mn^{2+}, indicating the possibility of dual ETs of Eu^{2+}→Tb^{3+} and Eu^{2+}→Mn^{2+}.

Figure 4a shows a series of emission spectra of SCBPO_Cl:0.05Eu^{2+}, $y$$Tb^{3+}$ (y = 0, 0.1, 0.2, and 0.3) under excitation at 365 nm. With increasing Tb^{3+} content, the emission intensities of Eu^{2+} at 450 nm decrease gradually, whereas the relative intensity of Tb^{3+} increases initially, before reaching a maximum at y = 0.3. Beyond this the Tb^{3+} intensity

dx.doi.org/10.1021/ic402870p | Inorg. Chem. 2014, 53, 3441−3448

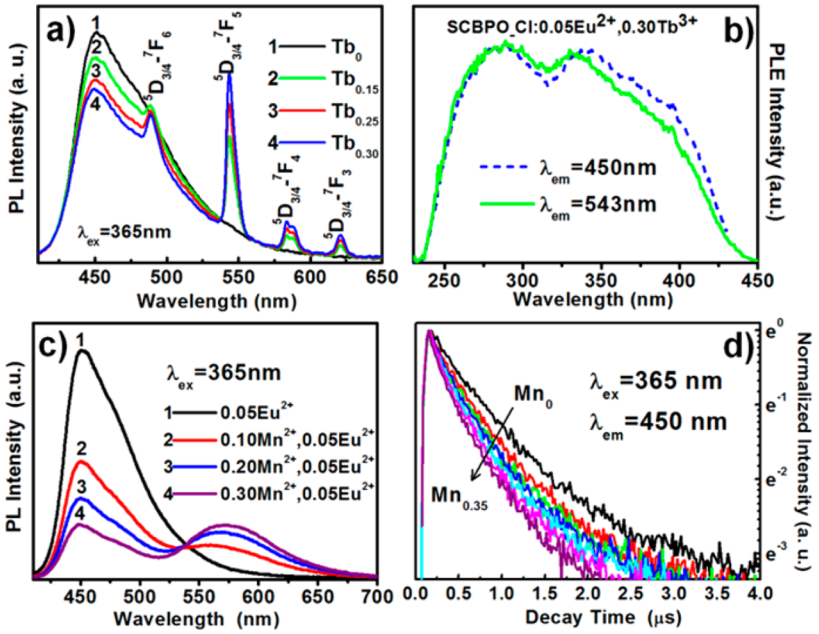

Figure 4. (a) The PL spectra of SCBPO_Cl:0.05Eu^{2+}, $y$$Tb^{3+}$ phosphors (y = 0, 0.15, 0.25, 0.30) under excitation at 365 nm. (b) The PLE spectra of SCBPO_Cl:0.05Eu^{2+}, 0.3Tb^{3+} sample by monitoring the emission at 450 and 543 nm. (c) The PL spectra of SCBPO_Cl:0.05Eu^{2+}, $z$$Mn^{2+}$ powders (z = 0, 0.1, 0.2, 0.3) under excitation at 365 nm. (d) The lifetimes of Eu^{2+} in SCBPO_Cl: 0.05Eu^{2+}, $z$$Mn^{2+}$ (z = 0, 0.1, 0.15, 0.20, 0.25, 0.30, 0.35).

decreases gradually, which is attributed to the results of Tb^{3+}–Tb^{3+} concentration quenching and the interaction between Eu^{2+} and Tb^{3+}. This result indicates that an ET occurs from Eu^{2+} to Tb^{3+}, which can be further confirmed from the PLE spectra (Figure 4b). Compared with the PLE spectra of a single Eu^{2+}-doped sample (λ_{em} = 450 nm), the appearance of a broad band transition from Eu^{2+} in the PLE spectrum, obtained by monitoring at 543 nm (Tb^{3+} emission), demonstrates the occurrence of an ET from Eu^{2+} to Tb^{3+}.[35] Figure 4c presents the PL spectra of SCBPO_Cl:0.05Eu^{2+}, $z$$Mn^{2+}$ (z = 0.1, 0.2, 0.3, and 0.4) under excitation at 365 nm. Analogously, the discussion in ET from Eu^{2+} to Mn^{2+} in SCBPO_Cl:0.05Eu^{2+}, $z$$Mn^{2+}$ powders is similar to that of SCBPO_Cl:0.05Eu^{2+}, $y$$Tb^{3+}$. Although the content of Eu^{2+} is fixed, the relative intensity of Eu^{2+} decreases gradually with increasing Mn^{2+} content due to the Eu^{2+}→Mn^{2+} ET. To further investigate the dynamic luminescence process between Eu^{2+} and Mn^{2+}, the PL decay curves of Eu^{2+} are measured, as shown in Figure 4d. The fluorescence of Eu^{2+} decays faster with increasing Mn^{2+} content. The decay process of these samples is characterized by an average lifetime, τ, which can be calculated using the following equation.[36,37]

$$\tau = \frac{\int_0^\infty I(t)t\,dt}{\int_0^\infty I(t)\,dt} \quad (1)$$

where $I(t)$ is the luminous intensity at time t. On the basis of equ 1, the luminescence lifetimes of Eu^{2+} are determined to be 1.234, 1.179, 1.161, 1.143, 1.137, 1.060, and 1.033 μs for the Mn^{2+} contents of 0, 0.1, 0.15, 0.2, 0.25, 0.3, and 0.35, respectively. The decrease in the lifetimes of Eu^{2+} with increasing Mn^{2+} content strongly demonstrates an ET from Eu^{2+} to Mn^{2+}. According to Paulose et al. ET efficiency (η_T) can be expressed as[38,39]

$$\eta_T = 1 - \frac{I_S}{I_{SO}} \quad (2)$$

where η_T is the ET efficiency and I_{so} and I_s are the luminescence intensity of a sensitizer in the absence and presence of an activator, respectively. As a consequence, the η_T values from Eu^{2+} to Mn^{2+} were calculated to be 0, 39.6%, 45.8%, 57.5%, 64.8%, 68.3%, and 78.2% for SCBPO_Cl:0.05Eu^{2+}, $z$$Mn^{2+}$ phosphors and plotted as a function of z (z = 0, 0.1, 0.15, 0.2, 0.25, 0.3, 0.35).

Figure 5 depicts the PL spectra of SCBPO_Cl:0.05Eu^{2+}, 0.3Tb^{3+}, 0.3Mn^{2+} and the corresponding PLE spectra

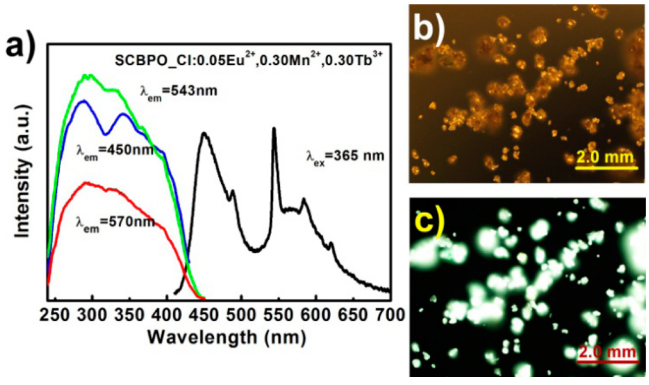

Figure 5. (a) The PL spectrum(right) of SCBPO_Cl:0.05Eu^{2+}, 0.3Tb^{3+}, 0.3Mn^{2+} phosphor and the corresponding PLE spectra(left) monitored the emission peaks at 450, 543, and 570 nm, respectively.

monitored at the emission peaks at 450 (Eu^{2+}), 543 (Tb^{3+}), and 570 nm (Mn^{2+}), respectively. Under excitation at 365 nm, the PL spectrum consists of three main emission bands in the visible-wavelength region, which are attributed to the contributions of Eu^{2+}, Tb^{3+}, and Mn^{2+}, as discussed above. Monitoring the emission of Eu^{2+} at 450 nm, the PLE spectrum exhibits a broad band in the range from 250 to 430 nm, which

dx.doi.org/10.1021/ic402870p | Inorg. Chem. 2014, 53, 3441−3448

is assigned to the 4f→5d characteristic transition of Eu^{2+}. It can be seen from Figure 5a that the profile of the PLE spectrum of 570 nm Mn^{2+} emission is consistent with that of Eu^{2+}, which means Mn^{2+} can be excited almost exclusively via the Eu^{2+} 4f→5d absorption, indicating the existence of ET from Eu^{2+} to Mn^{2+} in the triactivated SCBPO_Cl system.[33] Similarly, the appearance of broad-band transition of Eu^{2+} in the PLE spectrum of 543 nm Tb^{3+} emission suggests occurrence of ET from Eu^{2+} to Tb^{3+} in the triactivated SCBPO_Cl system. The direct excitation of Tb^{3+} is also possible by UV excitation at 365 nm, but the excitation strength is too weak relative to the sensitization way (Figure 3c). Therefore, we consider that white-light emission (λ_{ex} = 365 nm) from the SCBPO_Cl: $0.05Eu^{2+}$, $0.3Tb^{3+}$, $0.3Mn^{2+}$ phosphor consists mainly of the dual ETs of Eu^{2+}→Tb^{3+} and Eu^{2+}→Mn^{2+}. To demonstrate the photoluminescence characteristics of these microcrystalline powders, we also record the confocal microscope image (white-light illumination, dark-field mode) as well as the PL image of phosphor powders (excited with a 365 nm UV lamp), as shown in Figure 5b,c. From the PL image, a considerable number of phosphor particles, visible to the naked eye, show a bright white color luminescence (Figure 5c). These observations suggest that obtained white-light phosphor is not simple physical mixtures of the tricolor phosphors of SCBPO_Cl:Eu^{2+}/Tb^{3+}/Mn^{2+} but is a novel single-phased white-light phosphor SCBPO_Cl: $0.05Eu^{2+}$, $0.3Tb^{3+}$, $0.3Mn^{2+}$. In addition, the ETs from Eu^{2+} to Tb^{3+} and Mn^{2+} existing in SCBPO_Cl phosphors also suggest the phosphors are a single phase and not simple physical mixtures.

To prove the above assumption, the luminescence properties of white-light phosphor SCBPO_Cl: $0.05Eu^{2+}$, $0.3Tb^{3+}$, $0.3Mn^{2+}$ are further investigated by SEM image and μ-CL spectrum analysis. The SEM image and μ-CL spectrum recorded simultaneously from the same sample area are presented in Figure 6a. Similar to the PL results, blue (Eu^{2+}, 450 nm), green (Tb^{3+}, 542 nm), and orange-red (Mn^{2+}, 575 nm) emission bands are simultaneously found in the CL spectrum, which strongly demonstrates that a white-light emission is from the single-phased SCBPO_Cl: $0.05Eu^{2+}$, $0.3Tb^{3+}$, $0.3Mn^{2+}$ phosphor. Furthermore, it also suggests that white light can be realized in this triactivated SCBPO_Cl phosphor under low-voltage electron-beam excitation. The weak green and orange-red emission band relative to blue band is an artifact caused by weak sensitivity of PMT in the red region. To better the understanding of the luminescence properties of this single-phased white-light phosphor SCBPO_Cl: $0.05Eu^{2+}$, $0.3Tb^{3+}$, $0.3Mn^{2+}$ and its micro luminescence distribution, the monochromatic CL mappings of sample particle are collected at the wavelengths of 450, 542, and 575 nm, from an identical sample position, as shown in Figure 6b–d, respectively. On the basis of the three monochromatic CL mappings, which are recorded from the same scanning area at three different emission wavelengths, a uniform luminescence distribution of SCBPO_Cl:$0.05Eu^{2+}$, $0.3Tb^{3+}$, $0.3Mn^{2+}$ phosphor particle can be verified.

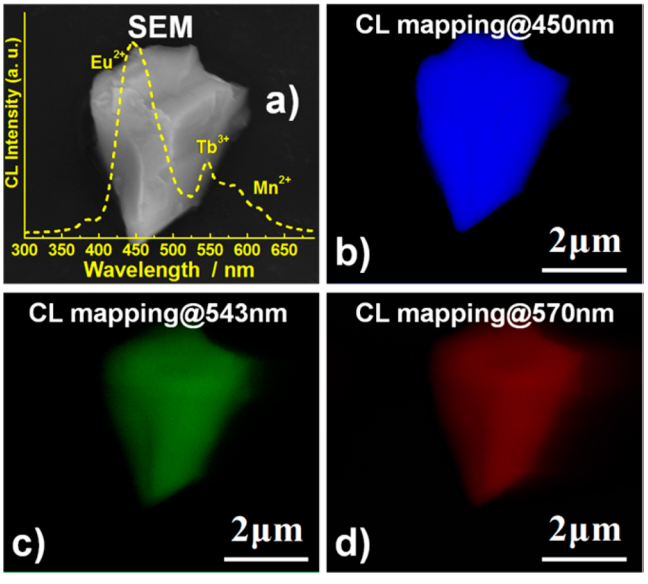

Figure 6. (a) The SEM image and CL spectrum collected simultaneously at the same area from SCBPO_Cl:$0.05Eu^{2+}$, $0.3Tb^{3+}$, $0.3Mn^{2+}$ sample. (b), (c), and (d) The corresponding monochromatic CL mappings (false color) taken at the wavelengths of 450, 542, and 575 nm, respectively.

According to the ET theory developed by Dexter,[40] the ET process through multipole interaction depends on the extent of overlap of the absorption and emission spectra of the sensitizer and activators.[41−43] In our case, the dual ET processes of Eu^{2+}→Tb^{3+} and Eu^{2+}→Mn^{2+} depends on the extent of spectral overlap between the PL band of Eu^{2+} and the absorption band of Tb^{3+} and Mn^{2+}. Figure 7 shows the PLE (λ_{em} = 450 nm) and PL (λ_{ex} = 365 nm) spectrum of SCBPO_Cl:$0.05Eu^{2+}$, $0.3Mn^{2+}$, $0.3Tb^{3+}$ phosphor and the corresponding energy level scheme of Eu^{2+}/Tb^{3+}/Mn^{2+}. To understand the dual ET processes of Eu^{2+}→Tb^{3+} and Eu^{2+}→Mn^{2+}, the possible ET routes are also shown in Figure 7 as a reference. These levels are determined from the PLE spectra (Figure 2) of Eu^{2+}, Tb^{3+}, and Mn^{2+} single-doped SCBPO_Cl samples as the excited states and from the PL spectrum of Tb^{3+} single-doped SCBPO_Cl sample as the ground-state splitting levels of terbium. As illustrated in Figure 7, the 5d band of Eu^{2+} overlaps partially the excited-state energy levels of Tb^{3+} ($^5L_6$/$^5D_3$) and Mn^{2+} (($^4T_1$ (^4G)/$^4T_2$ (^4D)). In addition, it can be seen that the lowest 5d energy level (~21 514 cm^{-1}) of Eu^{2+} is 938 cm^{-1} higher than the $^5D_4$ emitting energy level (~20 576 cm^{-1}) of Tb^{3+}. It was reported that the maximum vibration frequency for the SCBPO_Cl host was about 1000 cm^{-1}.[42] Therefore, the energy mismatch

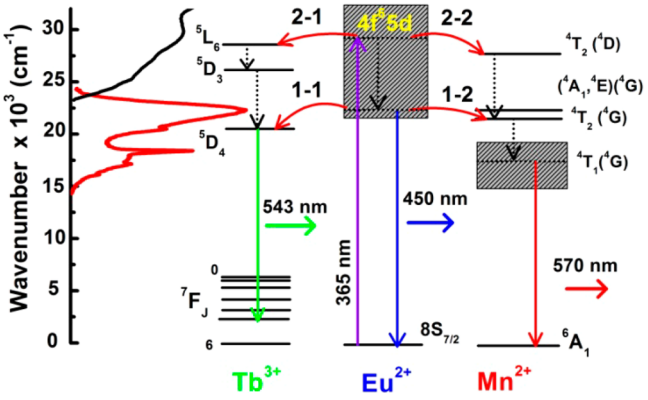

Figure 7. The energy levels schemes of Eu^{2+}/Tb^{3+}/Mn^{2+} and the possible the energy transfer modes for Eu^{2+}→Tb^{3+} and Eu^{2+}→Mn^{2+}. The PL (λ_{ex} = 365 nm, down) and PLE (λ_{em} = 450 nm, up) spectra of white-light emission phosphor SCBPO_Cl: $0.05Eu^{2+}$, $0.3Mn^{2+}$, $0.3Tb^{3+}$ are also shown as a reference.

dx.doi.org/10.1021/ic402870p | Inorg. Chem. 2014, 53, 3441−3448

between the lowest excited level of Eu^{2+} and the $^5D_4$ level of Tb^{3+} can be bridged by one phonon. Therefore, we consider that the dual-process ETs of $Eu^{2+}\rightarrow Tb^{3+}$ and $Eu^{2+}\rightarrow Mn^{2+}$ may take place in two ways: (1) The energy that populates the lowest 5d excited level of Eu^{2+} is transferred to the $^5D_4/^4T_2$ (^4G) emitting level of Tb^{3+}/Mn^{2+} by multiphonon relaxation (curved lines 1−1 and 1−2 of Figure 7), and then electrons in the excited-state energy level $^5D_4/^4T_2(^4G)$ return to the ground state $^7F_{6,\,5,\,4,\,3}/^6A_1$ by radiative transition. (2) The energy that populates the 5d excited level (~27 397 cm^{-1}) of Eu^{2+} by direct excitation at 365 nm is transferred from the $^5L_6/^4T_2(^4D)$ emitting level of Tb^{3+}/Mn^{2+} by multiphonon interaction (curved lines 2−1 and 2−2 of Figure 7), and then electrons in the excited-state energy level $^5L_6/^4T_2(^4D)$ return to the lowest excited level (Tb^{3+}, $^5D_4$; Mn^{2+}, $4T_1(^4G)$) and eventually to the ground state by radiative transition. All in all, a white-light emission is observed in the triactivated SCBPO_Cl system by utilizing the principle of the dual ETs.

One of the main purposes of this work is to explore the application potential of the studied phosphors. Therefore, we have studied the CIE values of selected SCBPO_Cl:0.05Eu^{2+}, $y$$Tb^{3+}$, $z$$Mn^{2+}$ phosphors. The CIE chromaticity coordinates for selected SCBPO_Cl:0.05Eu^{2+}, $y$$Tb^{3+}$, $z$$Mn^{2+}$ phosphors excited at 365 nm are calculated and presented in Table 1 and Figure 8.

Table 1. Representation of the CIE Chromaticity and QY for Selected SCBPO_Cl:$x$$Eu^{2+}$, $y$$Tb^{3+}$, $z$$Mn^{2+}$ Samples under Excitation at 365 nm

no.	composition	CIE (x, y)	quantum yield (QY)
1	0.30Tb^{3+}	(0.35, 0.56)	
2	0.30Mn^{2+}	(0.52, 0.48)	
3	0.05Eu^{2+}	(0.16, 0.17)	85.1%
4	0.05Eu^{2+}, 0.3Tb^{3+}	(0.19, 0.23)	72.7%
5	0.05Eu^{2+}, 0.3Mn^{2+}	(0.35, 0.35)	62.4%
6	0.05Eu^{2+}, 0.3Tb^{3+}, 0.1Mn^{2+}	(0.24, 0.25)	51.2%
7	0.05Eu^{2+}, 0.1Tb^{3+}, 0.3Mn^{2+}	(0.31, 0.32)	81.4%
8	0.05Eu^{2+}, 0.3Tb^{3+}, 0.3Mn^{2+}	(0.29, 0.30)	78.9%
9	0.05Eu^{2+}, 0.3Tb^{3+}, 0.5Mn^{2+}	(0.32, 0.33)	59.6%

As shown, the color tone of the phosphors shifts gradually from the blue (0.16, 0.17) to blue-greenish (0.19, 0.23) to white (0.32, 0.33) and eventually to warm-white (0.35, 0.35) by adjusting the content of Tb^{3+} and Mn^{2+}. The corresponding digital photographs under a 365 nm UV lamp are shown in the insets of Figure 8. These results clearly indicate that the color, tunable with content of Tb^{3+} and Mn^{2+}, makes these compositions promising candidates for WLEDs. In addition, the corresponding QY values measured under excitation at 365 nm are also listed in Table 1. It is found that the QY values decrease obviously with the introduction of Tb^{3+} and Mn^{2+}, which should be in relation to the energy loss in the $Eu^{2+}\rightarrow Tb^{3+}/Mn^{2+}$ ET process. As for the white-light phosphor SCBPO_Cl: 0.05Eu^{2+}, 0.3Tb^{3+}, 0.3Mn^{2+}, it is found that the QY can reach 78.9%, which is higher compared with some single-phased white-light emission phosphors reported to date.[44−46]

To evaluate the potential application of white-light SCBPO_Cl:0.05Eu^{2+}, $y$$Tb^{3+}$, $z$$Mn^{2+}$ phosphors, WLEDs were fabricated by combining a 400 nm NUVLED chip with a white-light phosphor that had an optimal composition. Figure 9 shows the electroluminescent spectrum of this fabricated

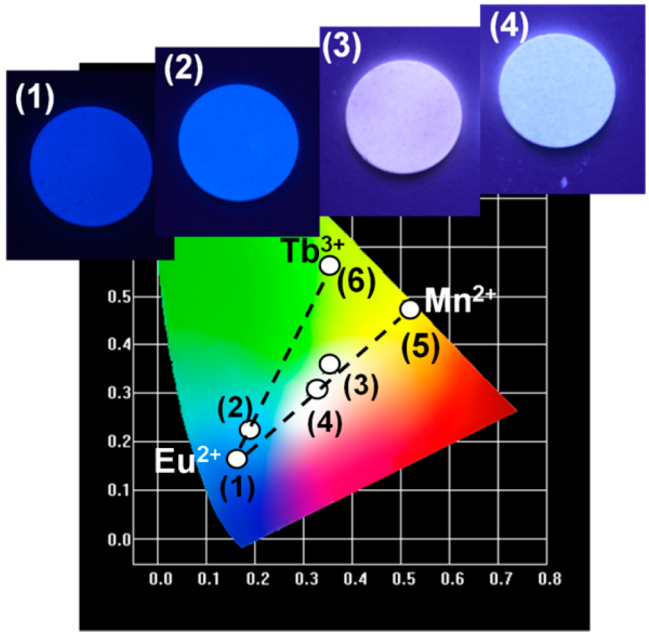

Figure 8. The CIE chromaticity coordinates of (1) SCBPO_Cl:0.05Eu^{2+}, (2) SCBPO_Cl:0.05Eu^{2+}, 0.3Tb^{3+}, (3) SCBPO_Cl:0.05Eu^{2+}, 0.3Mn^{2+}, (4) SCBPO_Cl:0.05Eu^{2+}, 0.3Tb^{3+}, 0.5Mn^{2+}, (5) SCBPO_Cl:0.3Mn^{2+}, and (6) SCBPO_Cl:0.3Tb^{3+} phosphors under excitation at 365 nm. The insets show the corresponding digital photos for selected samples upon excitation with a 365 nm UV lamp.

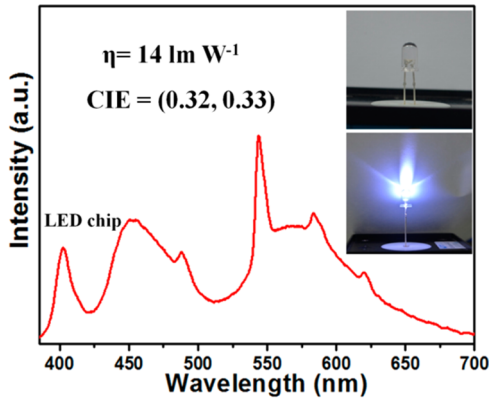

Figure 9. The electroluminescence spectrum of 400 nm NUVLED chip combined with white-light SCBPO_Cl: 0.05Eu^{2+}, 0.3Tb^{3+}, 0.5Mn^{2+} phosphor under the forward-bias current of 20 mA. The insets show the photographs of as-prepared WLED.

WLED, and the insets show the digital photos of a well-packed WLED. An ideal CIE coordinate (0.32, 0.33) of the WLED is obtained. The calculated luminous efficiency (η) for this WLED is 14 lm W^{1-} under a forward current of 20 mA and 3 V forward voltage. As far as we know, the obtained η is higher than that of some the same type of WLED devices, for example, $Ca_{2.34}Mg_{3.54}(PO_4)_4$:$Eu^{2+}{}_{0.06}$, $Mn^{2+}{}_{0.06}$(5.49 lm W^{1-}),[47] Na-$Ca_{0.96}BO_3$:0.01Ce^{3+}, 0.03Mn^{2+} (6.2 lm W^{1-}),[48] Sr_2Ba-$(AlO_4F)_{1-x}(SiO_5)_x$:Ce^{3+} (12 lm W^{1-}),[49] $KCaY(PO_4)_2$:Eu^{2+}, and Mn^{2+}(12.8 lm W^{1-}).[50] Even so, the relatively low η, compared to the commercial WLEDs (100 lm W^{1-}), is a consequence of the NUVLEDs being not as bright but having a larger Stokes shift. However, the relatively low η can be further improved through optimization of the processing conditions of the phosphors as well as device structure of the WLED. In

dx.doi.org/10.1021/ic402870p | Inorg. Chem. 2014, 53, 3441−3448

conclusion, these results show that this single-phased SCBPO_Cl:xEu^{2+}, yTb^{3+}, zMn^{2+} phosphor could be a promising white-light phosphor for NUVLEDs.

4. CONCLUSION

In summary, we have synthesized a series of Eu^{2+}, Tb^{3+}, Mn^{2+} triactivated (Sr_3, Ca, Ba)$(PO_4)_3Cl$ phosphors via high-temperature solid-state reactions and investigated their photoluminescence and μ-CL properties. Under excitation at 365 nm, a bright white light is realized in this triactivated SCBPO_Cl system by using the principle of dual ETs, for example, Eu^{2+}→Tb^{3+} and Eu^{2+}→Mn^{2+}. The ETs from Eu^{2+} to Tb^{3+} and from Eu^{2+} to Mn^{2+} in the SCBPO_Cl host are confirmed by photoluminescence excitation spectra and fluorescence decay dynamic analysis. Combining the analysis results of fluorescence images, CL spectra, and μ-CL mappings characteristic of a phosphor particle, a homogeneous luminescence distribution can be verified. Moreover, we demonstrated that the color hue for these single-phased white-light phosphors can be tuned from cool-white to middle-white and eventually to warm-white by simply controlling the content of Tb^{3+} and Mn^{2+}. The calculated luminous efficiency (η) of 14 lm W^{1-} and the CIE color coordinate of (0.32, 0.33) are realized by pumping this single-phased white-light phosphor with a 400 nm NUVLED chip. These results indicate that as-prepared white-emitting phosphor $(Sr_{3-x}Ca_{1-y-z}Ba)(PO_4)_3Cl$:$x$Eu^{2+}, yTb^{3+}, zMn^{2+} could be a promising single-phased phosphor for WLEDs.

■ ASSOCIATED CONTENT

Ⓢ Supporting Information

Further details about structure parameters of the ionic radii are given in Table S1. This material is available free of charge via the Internet at http://pubs.acs.org.

■ AUTHOR INFORMATION

Corresponding Authors

*E-mail: xtzhang@nenu.edu.cn. Phone/Fax: +86-431-85099772. (X.Z.).

*E-mail: daipp614@nenu.edu.cn. (P.D.).

Notes

The authors declare no competing financial interest.

■ ACKNOWLEDGMENTS

The work is supported by the National Natural Science Foundation of China (Grant No. 51072032, 41001258), the National Natural Science Young Foundation of (Grant No. 51302034, 11304035), the Program for New Century Excellent Talents in University (NECT-10-0320), the National Basic Research Program (2012CB933703), the Fundamental Research Funds for the Central Universities (Grant No. 12QNJJ007, 12SSXM001), and 111 project (No. B13013).

■ REFERENCES

(1) Hoppe, H. A. *Angew. Chem., Int. Ed.* **2009**, *48*, 3572−3582.

(2) Lin, C. C.; Liu, R.-S. *J. Phys. Chem. Lett.* **2011**, *2*, 1268−1277.

(3) Hartmann, P.; Pachler, P.; Payrer, E. L.; Tasch, S. *Proc. SPIE* **2009**, *7231*, 72310X.

(4) Wang, X. B.; Yan, X. S.; Li, W. W.; Sun, K. *Adv. Mater.* **2012**, *24*, 2742−7.

(5) Wen, D. W.; Dong, Z. Y.; Shi, J. X.; Gong, M. L.; Wu, M. M. *ECS J. Solid State Sci. Technol.* **2013**, *2*, R178−R185.

(6) Han, J. Y.; Im, W. B.; Lee, G. Y.; Jeon, D. Y. *J. Mater. Chem.* **2012**, *22*, 8793−8798.

(7) Lee, G. Y.; Han, J. Y.; Im, W. B.; Cheong, S. H.; Jeon, D. Y. *Inorg. Chem.* **2012**, *51*, 10688−94.

(8) Kido, J.; Shionoya, H.; Nagai, K. *Appl. Phys. Lett.* **1995**, *67*, 2281.

(9) Han, J. K.; Hannah, M. E.; Piquette, A.; Talbot, J. B.; Mishra, K. C.; McKittrick, J.; Ballato, J. *J. Am. Ceram. Soc.* **2013**, *96*, 1526−1532.

(10) Li, G. G.; Zhang, Y.; Geng, D. L.; Shang, M. M.; Peng, C.; Cheng, Z. Y.; Lin, J. *ACS Appl. Mater. Interfaces* **2012**, *4*, 296−305.

(11) Li, G. G.; Geng, D. L.; Shang, M. M.; Peng, C.; Cheng, Z. Y.; Lin, J. *J. Mater. Chem.* **2011**, *21*, 13334−13344.

(12) Shang, M. M.; Li, C. X.; Lin, J. *Chem. Soc. Rev.* **2014**, DOI: 10.1039/C3CS60314H.

(13) Bowers, M. J.; McBride, J. R.; Rosenthal, S. J. *J. Am. Chem. Soc.* **2005**, *127*, 15378−15379.

(14) Liao, Y.-C.; Lin, C.-H.; Wang, S.-L. *J. Am. Chem. Soc.* **2005**, *127*, 9986−9987.

(15) Wang, M.-S.; Guo, S.-P.; Li, Y.; Cai, L.-Z.; Zou, J.-P.; Xu, G.; Zhou, W.-W.; Zheng, F.-K.; Guo, G.-C. *J. Am. Chem. Soc.* **2009**, *131*, 13572−13573.

(16) He, G. J.; Guo, D.; He, C.; Zhang, X. L.; Zhao, X. W.; Duan, C. Y. *Angew. Chem., Int. Ed.* **2009**, *48*, 6132−5.

(17) Mao, Z. Y.; Wang, D. J. *Inorg. Chem.* **2010**, *49*, 4922−7.

(18) Mickens, M.; Assefa, Z.; Kumar, D. *J. Sol-Gel Sci. Technol.* **2012**, *63*, 153−161.

(19) Xia, Z. G.; Zhuang, J. Q.; Liu, H. K.; Liao, L. B. *J. Phys. D: Appl. Phys.* **2012**, *45*, 015302.

(20) Lorbeer, C.; Mudring, A.-V. *J. Phys. Chem. C* **2013**, *117*, 12229−12238.

(21) Zhang, Y.; Li, G. G.; Geng, D. L.; Shang, M. M.; Peng, C.; Lin, J. *Inorg. Chem.* **2012**, *51*, 11655−11664.

(22) Zhu, G.; Xin, S. Y.; Wen, Y.; Wang, Q.; Que, M. D.; Wang, Y. H. *RSC Adv.* **2013**, *3*, 9311.

(23) Huang, C.-H.; Chan, T.-S.; Liu, W.-R.; Wang, D.-Y.; Chiu, Y.-C.; Yeh, Y.-T.; Chen, T.-M. *J. Mater. Chem.* **2012**, *22*, 20210.

(24) Lu, W.; Guo, N.; Jia, Y. C.; Zhao, Q.; Lv, W. Z.; Jiao, M. M.; Shao, B. Q.; You, H. P. *Inorg. Chem.* **2013**, *52*, 3007−12.

(25) Lu, W.; Hao, Z. D.; Zhang, X.; Luo, Y. S.; Wang, X. J.; Zhang, J. H. *Inorg. Chem.* **2011**, *50*, 7846−51.

(26) Song, Y. H.; You, H. P.; Yang, M.; Zheng, Y. H.; Liu, K.; Jia, G.; Huang, Y. J.; Zhang, L. H.; Zhang, H. J. *Inorg. Chem.* **2010**, *49*, 1674−8.

(27) McKittrick, J.; Hannah, M. E.; Piquette, A.; Han, J. K.; Choi, J. I.; Anc, M.; Galvez, M.; Lugauer, H.; Talbot, J. B.; Mishra, K. C. *ECS J. Solid State Sci. Technol.* **2012**, *2*, R3119−R3131.

(28) Zeng, Q.; Liang, H. B.; Zhang, G. B.; Birowosuto, M. D.; Tian, Z. F.; Lin, H. H.; Fu, Y. B.; Dorenbos, P.; Su, Q. *J. Phys.: Condens. Matter* **2006**, *18*, 9549−9560.

(29) Nagpure, I. M.; Dhoble, S. J.; Mohapatra, M.; Kumar, V.; Pitale, S. S.; Ntwaeaborwa, O. M.; Godbole, S. V.; Swart, H. C. *J. Alloys Compd.* **2011**, *509*, 2544−2551.

(30) Dai, P. P.; Zhang, X. T; Bian, L. L.; Lu, S.; Liu, Y. C.; Wang, X. J. *J. Mater. Chem. C* **2013**, *1*, 4570.

(31) Nagpure, I. M.; Pitale, S. S.; Coetsee, E.; Ntwaeaborwa, O. M.; Terblans, J. J.; Swart, H. C. *Phys. B* **2012**, *407*, 1505−1508.

(32) Shang, M. M; Geng, D. L.; Yang, D. M.; Kang, X. J.; Zhang, Y.; Lin, J. *Inorg. Chem* . **2013**, *52*, 3102−12.

(33) Huang, C.-H.; Chen, T.-M. *J. Phys. Chem. C* **2011**, *115*, 2349−2355.

(34) Huang, C.-H.; Wu, P.-J.; Lee, J.-F.; Chen, T.-M. *J. Mater. Chem.* **2011**, *21*, 10489.

(35) Dai, P. P.; Zhang, X. T.; Zhao, H. H.; Wang, X. J.; Chen, X.; Li, C.; Lu, S.; Liu, Y. C. *ECS J. Solid State Sci. Technol.* **2013**, *2*, R213−R217.

(36) Guo, N.; Song, Y. H.; You, H. P.; Jia, G.; Yang, M.; Liu, K.; Zheng, Y. H.; Huang, Y. J.; Zhang, H. J. *Eur. J. Inorg. Chem.* **2010**, 4636−4642.

(37) Lahoz, F.; Martin, I. R.; Mendez-Ramos, J.; Nunez, P. *J. Chem. Phys.* **2004**, *120*, 6180−90.

(38) Paulose, P.; Jose, G.; Thomas, V.; Unnikrishnan, N.; Warrier, M. *J. Phys. Chem. Solids* **2003**, *64*, 841−846.
(39) Kwon, K. H.; Im, W. B.; Jang, H. S.; Yoo, H. S.; Jeon, D. Y. *Inorg. Chem.* **2009**, *48*, 11525−32.
(40) Dexter, D. L. *J. Chem. Phys.* **1953**, *21*, 836.
(41) Hu, S. S.; Tang, W. J. *J. Mater. Sci.* **2013**, *48*, 5840−5845.
(42) Zhang, Z.; Wang, J.; Zhang, M.; Zhang, Q.; Su, Q. *Appl. Phys. B: Lasers Opt.* **2008**, *91*, 529−537.
(43) Guo, N.; Huang, Y. J.; You, H. P.; Yang, M.; Song, Y. H.; Liu, K.; Zheng, Y. H. *Inorg. Chem.* **2010**, *49*, 10907−13.
(44) Guo, N.; Jia, Y. C.; Lu, W.; Lv, W. Z.; Zhao, Q.; Jiao, M. M.; Shao, B. Q.; You, H. P. *Dalton Trans.* **2013**, *42*, 5649−54.
(45) Li, G. G.; Geng, D. L.; Shang, M. M.; Zhang, Y.; Peng, C.; Cheng, Z. Y.; Lin, J. *J. Phys. Chem. C* **2011**, *115*, 21882−21892.
(46) Lv, W. Z; Lu, W.; Guo, N.; Jia, Y. C; Zhao, Q.; Jiao, M. M.; Shao, B. Q.; You, H. P. *Dalton Trans.* **2013**, *42*, 13071−7.
(47) Kwon, K. H.; Im, W. B.; Jang, H. S.; Yoo, H. S.; Jeon, D. Y. *Inorg. Chem.* **2009**, *48*, 11525−11532.
(48) Sun, J. F.; Lian, Z. P.; Shen, G. Q.; Shen, D. Z. *RSC Adv.* **2013**, *3*, 18395.
(49) Denault, K. A.; George, N. C.; Paden, S. R.; Brinkley, S.; Mikhailovsky, A. A.; Neuefeind, J.; DenBaars, S. P.; Seshadri, R. *J. Mater. Chem.* **2012**, *22*, 18204.
(50) Liu, W. R.; Huang, C. H.; Yeh, C. W.; Tsai, J. C.; Chiu, Y. C.; Yeh, Y. T.; Liu, R. S. *Inorg. Chem.* **2012**, *51*, 9636−41.